Electrode-modified zeolites: electrode microstructures contained in and on a heterogeneous catalyst

ARTICLE *in* THE JOURNAL OF PHYSICAL CHEMISTRY · JULY 1989

Impact Factor: 2.78 · DOI: 10.1021/j100351a040

3 AUTHORS, INCLUDING:

Walter E Rudzinski
Texas State University
76 PUBLICATIONS **3,001** CITATIONS

OFFICE OF NAVAL RESEARCH

Contract N00014-83-K-0470-P00003

R&T Code NR 33359-718

Technical Report No. 115

Electrode-Modified Zeolites - Electrode Microstructures Contained In and On a Heterogeneous Catalyst

by

D.R. Rolison, E.A. Hayes, R.J. Nowak, S. Pons and M. Fleishmann

Prepared for publication in J. Phys. Chem.

Department of Chemistry
University of Utah
Salt Lake City, UT 84112

July 15, 1988

SECURITY CLASSIFICATION OF THIS PAGE

REPORT DOCUMENTATION PAGE

1a. REPORT SECURITY CLASSIFICATION: Unclassified	1b. RESTRICTIVE MARKINGS
2a. SECURITY CLASSIFICATION AUTHORITY	3. DISTRIBUTION / AVAILABILITY OF REPORT: Approved for public release and sale. Distribution unlimited.
2b. DECLASSIFICATION / DOWNGRADING SCHEDULE	
4. PERFORMING ORGANIZATION REPORT NUMBER(S): ONR Technical Report No. 115	5. MONITORING ORGANIZATION REPORT NUMBER(S)
6a. NAME OF PERFORMING ORGANIZATION: University of Utah; 6b. OFFICE SYMBOL (If applicable)	7a. NAME OF MONITORING ORGANIZATION
6c. ADDRESS (City, State, and ZIP Code): Department of Chemistry, Henry Eyring Building, Salt Lake City, UT 84112	7b. ADDRESS (City, State, and ZIP Code)
8a. NAME OF FUNDING / SPONSORING ORGANIZATION: Office of Naval Research; 8b. OFFICE SYMBOL (If applicable)	9. PROCUREMENT INSTRUMENT IDENTIFICATION NUMBER: N00014-83-K-0470-P00003
8c. ADDRESS (City, State, and ZIP Code): Chemistry Program, Code 1113, 800 N. Quincy Street, Arlington, VA 22217	10. SOURCE OF FUNDING NUMBERS: PROGRAM ELEMENT NO. / PROJECT NO. / TASK NO. / WORK UNIT ACCESSION NO

11. TITLE (Include Security Classification): Electrode-Modified Zeolites - Electrode Microstructures Contained In and On a Heterogeneous Catalyst

12. PERSONAL AUTHOR(S): D.R. Rolison, E.A. Hayes, R.J. Nowak, S. Pons and M. Fleishmann

13a. TYPE OF REPORT	13b. TIME COVERED	14. DATE OF REPORT (Year, Month, Day)	15. PAGE COUNT
Technical	FROM 9/87 TO 7/88	July 15, 1988	24

16. SUPPLEMENTARY NOTATION

17. COSATI CODES			18. SUBJECT TERMS (Continue on reverse if necessary and identify by block number)
FIELD	GROUP	SUB-GROUP	zeolites, microelectrodes

19. ABSTRACT (Continue on reverse if necessary and identify by block number)

Attached.

20. DISTRIBUTION / AVAILABILITY OF ABSTRACT	21. ABSTRACT SECURITY CLASSIFICATION
☒ UNCLASSIFIED/UNLIMITED ☐ SAME AS RPT ☐ DTIC USERS	Unclassified
22a. NAME OF RESPONSIBLE INDIVIDUAL: Stanley Pons	22b. TELEPHONE (Include Area Code): (801)581-4760; 22c. OFFICE SYMBOL

DD FORM 1473, 84 MAR — 83 APR edition may be used until exhausted. All other editions are obsolete.

SECURITY CLASSIFICATION OF THIS PAGE

Abstract

In this work, zeolite-supported Pt(0) microstructures sized less than 10 nm are accessed as electrodes using dispersion electrolysis. Modification of an heterogeneous catalyst with ultramicroelectrodes permits exploration of electrode processes in an interphase dominated by the nature of the heterogeneous catalyst and at electrode sizes where bulk metallic properties may not apply. The systems described are Pt supported on zeolite Type Y and Pt supported on gamma-alumina.

The electrolytic response of zeolite-supported Pt in the absence of added electrolyte salt for water or benzene:water is markedly more effective than that at alumina-supported Pt and is seen to depend on the size of the Pt particles supported on the exterior of the zeolite surface. Both supported systems behave as ultramicroelectrodes in that electrolysis is sustained in their presence under conditions that are strictly ohmic for the feeder electrodes due to the high resistivity of the media in the absence of electrolyte salt. X-ray photoelectron spectroscopic measurements confirm the expected low external surface concentration of Pt on the zeolite and indicate approximate particle size of the supported Pt

ELECTRODE-MODIFIED ZEOLITES - ELECTRODE MICROSTRUCTURES CONTAINED IN AND ON AN HETEROGENEOUS CATALYST

Debra R. Rolison*, E. A. Hayes, and R. J. Nowak+
Code 6170, Surface Chemistry Branch
Naval Research Laboratory
Washington, DC 20375-5000

Stanley Pons
Department of Chemistry
University of Utah
Salt Lake City, UT 84112

Martin Fleischmann
Department of Chemistry
The University
Southampton SO9 5NH, England

* Author to whom correspondence should be addressed
+ Permanent address: Code 1113ES, Office of Naval Research,
800 N. Quincy Street, Arlington, VA 22217-5000

Introduction

Manipulation of the environment in which electrode processes occur underlies the research on chemically modified electrodes and to some extent, the research on ultramicroelectrodes. Chemically modified electrodes are designed to impart a chemically specific environment at the electrode surface [1], while ultramicroelectrodes shrink the electrode size to the extent that electrode processes may be studied at shorter times or in unconventional media [2,3]. Ultramicroelectrodes, conductive materials with one dimension less than 1 μm, also are of interest for their analytical possibilities [2,3].

Recent work has combined these two approaches of controlling the electrochemical interphase, e.g., the polymer modification of ultramicroelectrode surfaces [4,5]. An alternate means to devise a microelectrode/chemically specific interphase is to form the microelectrode within a well defined chemical structure. Our approach is the latter and relies on the crystalline aluminosilicate zeolites [6]. These materials offer advantages on both accounts - as a support and template for the microelectrode and as a chemical environment with inherent interest for the study of electrode processes.

Most intriguing from the viewpoint of chemical modification of the electrochemical interphase is the character of the zeolite support itself and possible interactions that may arise when electrodes are structured within an heterogeneous catalyst with the chemical and architectural nature of a zeolite. Zeolites are one type of an inorganic lattice that has been formed or placed on electrode surfaces to perturb electrochemical processes [7-14].

Most zeolites exhibit molecular sieving properties arising from the channel, pore, and cage structure of the lattice [15]. In addition, the aluminosilicate lattice has fixed anionic sites counterbalanced by cations, many of which are

exchangeable. The versatile cation-exchange nature of zeolites allows a great range of metal ions and complexes to be loaded on the zeolite. Applying the appropriate redox chemistry to these exchanged metal ions or complexes produces metal or metal oxide microstructures while the internal architecture of the zeolite limits the ultimate particle size of the formed microstructure.

The fabrication of ultramicroelectrodes is often technically difficult or may require advanced technology, e.g., microlithography [3]. Exploiting the advantages of ultramicroelectrodes in a macroscopic manner, such as for electrosynthesis, requires electrode structures containing multiple microelectrode sites. The synthesis of zeolite-supported metal or metal oxide microstructures resolves both issues simply since a relatively straightforward preparation yields multiple ultramicroelectrode sites per zeolite particle.

Metal and metal-oxide microstructures supported on zeolites are well documented, as are the synthetic procedures to prepare them [16]. Metal microstructures constrained within the supercages of zeolites can range in size from single atoms to particles on the order of 1-2 nm. The surface area of a zeolite is primarily internal or intracrystalline, so, only a small fraction of metal is supported on the exterior of the zeolite [15,16]. Particles formed on exterior, although not constrained by the internal architecture of the zeolite still much smaller than the micrometer size of most ultramicroelectrodes [3].

In common with other ultramicroelectrodes, electrical contact must be made the microscopic conducting material. Pons, et. al., have demonstrated that free standing microelectrodes can be used for practical electrosynthetic purposes by applying bipolar electrolytic conditions to dispersions consisting of low concentrations of metal spheres with radii on the order of 10^{-5} to 10^{-3} cm (10 μm) [17,18]. Such dispersions differ from typical monopolar and bipolar flu

bed electrodes which contain high concentrations of particles in the size range 0.005-0.5 cm [19-21] and may be likened to the use of colloidal metals (typically sized at 10^{-6} cm (10 nm)) at the mixture potential of two redox couples [22,23] or in photoelectrolysis [24-34].

The use of bipolar dispersions between feeder electrodes permits other types of conducting materials to be accesssed as ultramicroelectrodes, e.g., colloidal conductors or semiconductors, or as we describe in this paper, supported metal microstructures. The use of dispersed zeolite-supported ultramicroelectrodes enables a practical, three-dimensional exploration of the interplay of molecular-size control with electrochemical control and allows a wide range of metals and metal oxides to be explored as ultramicroelectrodes, thus extending the diversity of ultramicroelectrode systems.

Exploiting the templating ability of a zeolite to form metal microstructures 1 nm in size within the zeolite offers electrochemists a chance to explore the electrochemical reactivity and character of metals at sizes where bulk metallic properties may not be exhibited. Furthermore, electrolyses are now allowed using loadings of catalysts which are one-to-two orders of magnitude below those which have so far been achieved (typically 3 mg cm^{-3}) [6,17,18].

Another possible benefit of structuring the electrode at the zeolite lies the ionic nature of the material; zeolites are modeled as a concentrated electrolyte, solid-state solvent system [15]. Electrode processes occuring at zeolite-supported electrode sites may seemingly occur in a high ionic strength interphase. In the dispersion experiment, in the absence of (soluble) supporting electrolyte, a zeolite-supported ultramicroelectrode may act as a mobile solid electrode/electrolyte package.

The results presented in this paper demonstrate that Pt supported on al-

and Pt supported on Type Y zeolite (Pt-Y) exhibit the characteristics of ultramicroelectrodes when used as dispersed electrodes and that marked differences result when the support is zeolite rather than alumina. X-ray photoelectron spectroscopy (XPS) verifies the low loading of metal on the zeolite exterior and indicates the small particle sizes of Pt supported on the exterior.

Experimental

Preparation of Pt-Y

Gallezot and co-workers have developed synthetic procedures for the formation, location, and sizing of Pt in Pt-Y [35]. Pt is introduced into the sodium form of Type Y zeolite (NaY) by ion exchange of $Pt(NH_3)_4^{2+}$ for Na^+ to form a mixed ionic species (designated as PtY). For the dispersion experiments 1, 5, and 10% weight loadings of Pt were chosen. 10.00 g of Type Y powder (Strem Chemicals; sieved to <44 μm), previously equilibrated to constant weight over saturated NH_4Cl, was stirred for 24 h in 250 ml of 2.05 mM, 500 ml of 5.13 mM, and 1 l of 5.13 mM $Pt(NH_3)_4Cl_2$ (Aesar) to prepare weight loadings of 1, 5, and 10% PtY, respectively. The suspension was filtered and the solid resuspended in water until the filtrate tested negatively for Cl^- with $AgNO_3$; PtY was then dried at 135°C. Equilibrium exchnge occurs at these low weight loadings, so, essentially 100% of the Pt exchanges. An aliquot of the initial filtrate from each exchange was analyzed by DC plasma spectroscopy for Pt and confirmed that greater than 99% exchange occured in all cases.

In Gallezot's procedure, PtY is heated in flowing oxygen to evolve NH_3 and place the Pt in a more readily reducible form; this step is also crucial in determining the final distribution and size of Pt particles within the zeolite [35]. Activation at 300°C places most of the Pt ions in the supercages of the zeolite, while oxygen activation at 600°C strews the Pt ions throughout the

zeolite, even into the smaller sodalite cages. After reduction at 300° with flowing hydrogen, 0.6-1.3 nm Pt particles, which remain in the supercages, are reported for the material activated at 300°, while 1.5-2 nm Pt particles form in the bulk of the zeolite crystal of the material activated at 600°. For our work, only 1% PtY was activated at both temperatures; these systems are designated as 1% $Pt\text{-}Y_{300}$ or 1% $Pt\text{-}Y_{600}$.

PtY was spread as a thin layer in two ceramic boats and loaded in a tube furnace at either 240°C or 420°C under a flow of O_2. The temperature was raised over 1 h to either 300° or 600° and maintained for 1 h. For all samples, the system was purged with helium for 10-20 min before H_2 was introduced; reduction was run at 300° for >12 h for all activated weight loadings. The system was then evacuated and held at 300° for 2 h.

After reduction with hydrogen, H^+ is present as a counterion in the zeolite. To minimize the acidity, all Pt-Y samples were stirred for 24 h in 100 ml of 0.1 M NaCl to ion exchange Na^+ for accessible H^+. The solid was then resuspended in H_2O and filtered until the filtrate again tested negatively for Cl^-. The samples were dried at 70-135°C before use as dispersed electrodes.

PtY and Pt-Y samples were analyzed using a Surface Science/UHV Instrument X-ray photoelectron spectrometer with an Al anode to assess the surface abundance of Pt on the zeolite after ion exchange and after redox chemistry. Samples were prepared for analysis by pressing a thin film of the powder in indium foil; In3d photoelectrons were not observed in 0-1000 eV survey scans.

The use of indium helped to minimize charging; even with this precaution the ion-exchanged materials (PtY) experienced greater charging difficulties than did the metal-loaded samples. Binding energies are referenced to trace, adventitious carbon (C1s = 284.6 eV). Suib and co-workers have recently

discussed the preferred use of the Na $KL_{23}L_{23}$ transition as the binding energy reference for zeolites with Si/Al < 5 [36], a category which includes Type Y zeolite. In this study, a high resolution scan of the Na $KL_{23}L_{23}$ region (497.6 eV [36]) was not performed, however, multiple (2-4) analyses were run for each sample to establish error limits on the quantitative analysis of the XPS data. Using C1s as reference for 19 samples of NaY, PtY, and Pt-Y yielded a binding energy of 102.7±0.2 eV for Si2p, in excellent agreement with the value for NaY previously reported by Suib, et al. [37].

When multiple peaks were present, the envelope was deconvolved using a chi-squared minimization calculation. Peak positions, heights, and widths were first assigned by graphic editing. The binding energy difference between the 7/2 and 5/2 lines of the Pt4f doublet was constrained after a minimized fit was obtained and then re-fit for final results. The relative area of an elemental line is corrected for cross-sectional and instrumental factors. Analyses were performed at pressures < 5 x 10^{-9} torr.

Dispersion Experiments

The cell used for dispersion electrolysis has been described previously [1]. Briefly, the cell is formed between two concentric cylindrical Pt foils with a [illegible] of 0.5 cm and a height of 5 cm. One foil is wrapped around the inner wall of a fritted (medium porosity) glass tube with an inlet for the dispersing gas below the frit. The second Pt foil is wrapped around the outside of a glass finger is inserted into the fritted tube to form the cell. The electrode particles are dispersed in the electrolysis solution with a rapid flow of helium or nitrogen. The volume of the assembled cell is approximately 35 ml and the facial surface of the feeder electrodes is 85 cm^2. The design of this electrolysis cell coincidentally provides a conductivity cell; the toroidal geometry yields a

calculated cell constant that agrees exactly with the value determined using 0.1M KCl (0.1 cm^{-1}).

Solvents were high impedance water (obtained either by triple distillation over $KMnO_4$ or from a Millipore system) or a two-phase mixture of benzene (Fisher, reagent grade) and high impedance water. 1% Pt on high purity gamma-alumina (Aesar, designated as 1% Pt/Al_2O_3) or Pt-Y in 25 or 100 mg amounts was stirred in the solvent to produce a suspension before addition to the cell. Unlike previous experiments in benzene:water with Pt microspheres or graphite powder [38], the alumina- and zeolite-supported Pt associated primarily with the water phase. This is probably due to the highly polar nature of the supports, whereas the less polar unsupported Pt and graphite preferred the nonpolar benzene phase. No electrolyte salts were added for any of the electrolyses.

All electrolytic experiments were performed with the cell thermostatted at 0-5°C. A DC power supply (Kepco Models HB-6 or CK-36) was used to vary the voltage between the feeder electrodes. The Pt foil wrapped around the finger insert was biased as the cathode for these experiments. Current was calculated from the output voltage dropped across a precision 0.39 or 1.00 ohm resistor. Voltages were measured with a dual-channel electrometer (Keithley Model 619). Current values were noted when a steady-state response was achieved after each change in applied voltage. Current-voltage (i-V) values were obtained with each increase in applied voltage, until the current passed was too high for the power supply to maintain regulated voltage, and then again as the applied voltage was lowered to 0 V. The process was repeated for some experiments. The time required to reach a steady-state response increased as the applied voltage increased and was on the order of minutes at the higher voltages.

The Pt feeder electrodes and the glass portions of the cell were cleaned

hot 1:1 HNO_3:H_2SO_4 and copiously rinsed and sonicated in high impedance water. After cleaning the cell, a i-V curve was obtained for the feeder electrodes in high impedance water; the first run always produced higher currents than subsequent runs with fresh aliquots of H_2O, which yielded low and comparable values.

Results and Discussion

Dispersion Electrolysis with Benzene:Water

Figure 1 illustrates the i-V curves that are obtained when supported Pt ultramicroelectrodes are used for the dispersion electrolysis of the two-phase system of benzene and water. The response for the feeder electrodes alone (Figure 1D), in the absence of any dispersed microelectrodes, is indistinguishable from a zero current response when plotted on the scale of Figure 1, e.g., < 1 mA of current flowed at 300 V/cm. The i-V curve obtained for 0.1 g dispersed 1% Pt/Al_2O_3 (Figure 1B) exhibits a response comparable to that observed for 0.1 g of dispersed Pt microspheres in this medium [18,38].

The first point of importance is that negligible electrolysis can be supported by the feeder electrodes alone in this low dielectric medium. The second point is that the curvature, the non-ohmic response, above 100 V/cm for Figure 1B indicates that electrolysis will occur even when the Pt microparticles are supported and not freely rotating microspheres. As anticipated, larger currents are obtained with the mass of supported dispersed particles - and thus the number and available surface area of electrodes - is increased: compare Figure 1B (100 mg of 1% Pt/Al_2O_3) and Figure 1C (26 mg of 1% Pt/Al_2O_3).

Substituting 1% Pt-Y_{300} as the dispersed electrode produces a markedly enhanced i-V curve, so that larger currents are obtained at any given voltage relative to 1% Pt/Al_2O_3. This would appear to be a clear example of support differences since the weight loading of Pt is the same for both the alumina and

zeolite systems. An intriguing complication arises due to the nature of these supports. Gamma-Al_2O_3 was chosen as a non-zeolite support of comparable high surface area (300 m^2/g for the alumina), but as >90% of the surface area of zeolite is internal [15,16], most of the Pt supported "on" Pt-Y is found within the zeolite. Thus, externally sited and physically accessible Pt on 1% Pt-Y is expected to be on the order of 0.1 wt%, while most of the Pt particles on 1% Pt/Al_2O_3 are expected to be physically accessible to the feeder electrodes and to Pt sited on other alumina particles. High surface area Al_2O_3 is porous, so some of the Pt particles may be screened from direct physical contact, but not to the extent of the zeolite. If only physically accessible Pt, i.e., Pt sited on the exterior surface of the support, responds electrochemically, this would imply that dispersion electrolysis is remarkably more effective at Pt formed on zeolite than at Pt formed on Al_2O_3. The nature of externally sited Pt particles on zeolite Y can be explored by X-ray photoelectron spectroscopy (XPS).

X-ray Photoelectron Spectroscopic Analysis of Supported Pt

$Pt4f_{7/2}$ is the strongest line for Pt, but surface concentrations are low for these samples and analysis is further complicated by the Al2p line as a near neighbor. Figure 2 shows that the Pt4f-Al2p region can still be quite useful, both qualitatively and quantitatively. The Pt4f-Al2p envelope offers an immediate gauge of the oxidation state of the Pt. For the ion-exchanged samples, where Pt is present as Pt(II), the $Pt4f_{7/2}$ line lies obscured by the Al2p line; however, the Pt $4f_{5/2}$ line, which lies 3.4 eV above the $Pt4f_{7/2}$ line [39], is clearly seen as a shoulder on the high binding energy side of the Al-$Pt4f_{7/2}$ envelope. Figure 2, Curves A and B show the resolved Pt $4f_{5/2}$ line for the 1 and 5% PtY samples. Upon oxidation-reduction to form Pt(0), the $Pt4f_{5}$ line is obscured, while the $Pt4f_{7/2}$ line is clearly seen on the the low binding energy side of Al2p, even for a 1% loading (Figure 2C).

The more cleanly resolved half of the Pt4f doublet was used for quantitation: $Pt4f_{5/2}$ for the ion-exchanged materials and $Pt4f_{7/2}$ for the metal-loaded samples. These numbers were cross-checked and found to be in good agreement with the relative areas determined for the other half of the Pt4f doublet (as obtained from deconvolution of the Pt4f-Al2p envelope) and for the $Pt4d_{5/2}$ line. A binding energy of 73.3±0.5 eV (9 samples) for $Pt4f_{7/2}$ in the ion-exchanged materials was calculated using the determined position of the Pt $4f_{5/2}$ minus the known separation of the 5/2 from the 7/2 in the Pt4f doublet. This value is in good agreement with the literature number for divalent Pt in such compounds as $PtCl_2$ and $K_2Pt(CN)_4$ [39]. The binding energy for $Pt4f_{7/2}$ in the metal-loaded materials, 71.5±0.5 eV (9 samples), is in accord with the literture value of 70.9 eV for bulk metallic Pt and in good agreement with Pt as Pt(0) in triphenylphosphine complexes [39]. As implied by the electrolytic response, and confirmed by the XPS data, Pt supported on Pt-Y has been placed in a metallic form following the redox chemistry.

The concentration of Pt on the zeolite exterior can be tracked by either the ratio of the relative areas of Pt4f to Si2p or the calculated relative atom percent of Pt; both numbers are included in Table I. Ion exchange is an equilibrium process, so a uniform distribution of the Pt(II) ion should result; this is affirmed by the XPS data. Normalizing to the values for the 1% loading yields for the Pt:Si ratio the series 1:4.6:10.3, which agrees quite well with the expected series of 1:5:10. Using values obtained for the relative atom percent of Pt yields the series of 1:4.6:11.2. Thus, XPS provides a reliable indication of the true surface concentration of Pt for the ion-exchanged samples. The low relative atom percent of Pt obtained for these samples confirms the expected low external surface concentration of Pt on the ion-

exchanged form and agrees with the anticipated predominance of the Pt loading within the zeolite interior.

Table I also contains two parameters used to track the state of the zeolite following ion exchange and redox reactions. The difference in binding energies between O1s and Si2p is characteristic of the zeolite lattice and remains invariant within experimental error for all zeolite samples. In addition, the relative area ratio of O1s:(Si2p + Al2s) remains equal to 2.0 as predicted by the ideal formula for faujasite Type Y: $Na_{56}[(AlO_2)_{56}(SiO_2)_{136}]$ [15]. These results indicate that at the Pt loadings used in this study, no gross changes have occurred in the nature of the zeolite after ion-exchange or redox chemistry.

The quantitative indicators for Pt for 1% Pt-Y_{300} are identical to those for 1% Pt-Y_{600}, see Table I, and are averaged to obtain a representative set of values for 1% Pt-Y. Although the particle sizes formed within the zeolite can differ by a factor of two based on these temperatures of oxygen activation [35], externally sited Pt particles do not benefit from the intracrystalline architecture of the zeolite. Similarly sized particles should form on the exterior of these two types of 1% weight-loaded samples since the nature and concentration of exterior-sited Pt(II) remains unchanged.

The relative atom percent of Pt visible via XPS increased from 0.08±0.02% 1% PtY to 0.12±0.01% for 1% Pt-Y; as these numbers are essentially identical, demonstrates that massive migration of Pt from the zeolite interior to the ex does not occur during oxygen activation or hydrogen reduction of 1% weight-lo samples. It further indicates that after redox chemistry, the Pt particles wh form on 1% Pt-Y are sufficiently small so that photoelectrons generated at Pt the interior of these particles are not screened. The particle sizes <u>on the zeolite exterior</u> must then be on the order of the escape depth of a

photoelectron, 2.5-5 nm, or smaller.

At weight loadings greater than 1%, the redox chemistry necessary to convert Pt(II) sites to Pt(0) affects the surface concentration of Pt as is evident from the Pt concentration indicators in Table I. The Pt:Si series normalized to 1% Pt-Y is now 1:2.9:4.5 (1:2.8:4.8 if the numbers for the relative atom percent of Pt are used), significantly different than the expected 1:5:10.

This diminishment of Pt concentration at the higher loadings is most probably due to the formation of particles of Pt on the zeolite exterior that are sufficiently large to mask some of the Pt, i.e., the particles have a diameter greater than the escape depth of a Pt photoelectron. This loss of Pt intensity is unlikely to be due to Pt(0) migrating to the inside of the zeolite during oxidation-reduction. Particles sized significantly greater than 2.5 nm for 5 and 10% Pt-Y would also explain the greater relative decrease in surface Pt for 10% Pt-Y; aggregation into even larger particles at the zeolite exterior during oxidation-reduction should be favored as the Pt ion concentration (i.e., weight loading) increases. The XPS results indicate that the particles formed on the exterior of 10% Pt-Y are larger than those formed on the exterior of 5% Pt-Y

Alumina vs. Zeolite as an Ultramicroelectrode Support

The XPS results for 1% Pt/Al_2O_3 show that Pt is in a metallic form and the Pt particle size on this support is significantly greater than the escape of the photoelectrons as a relative atom percent of only 0.3 was obtained. Some of the smallest Pt particle sizes supported on high surface area alumina on the order of 15 nm [40], the XPS-derived conclusion that Pt on our commercial sample of 1% Pt/Al_2O_3 is sized at several tens of nanometers while exterior Pt on 1% Pt-Y is sized at several nanometers seems quite reasonable. The order of exterior-sited particle sizes among our supported Pt samples, from XPS, follows

order:

$$1\%\ Pt\text{-}Y_{300} = 1\%\ Pt\text{-}Y_{600} \ll [5\%\ Pt\text{-}Y < 10\%\ Pt\text{-}Y],\ 1\%\ Pt/Al_2O_3.$$

The question now becomes what is the origin of the great difference in electrolytic current observed in Figure 1 for 1% Pt-Y and 1% Pt/Al_2O_3. The XPS data show that the size of externally sited particles differs between 1% Pt-Y and 1% Pt/Al_2O_3 - does 1% Pt-Y with a greater number of smaller particles have greater electrode area to yield more current, although current densities may be similar at both systems? Table II lists the calculated surface areas for a range of spherical particles of Pt; these numbers reinforce the efficacy of using supported metal particles sized significantly below 100 nm as dispersed electrodes. 1% Pt/Al_2O_3, with an estimated particle size between 10 and 10^2 nm, supports a comparable magnitude of electrolysis as unsupported Pt microspheres, but by using 10^2-times less Pt.

Externally sited Pt on 1% Pt-Y, although smaller in size than Pt on 1% Pt/Al_2O_3, has a lower surface concentration due to the nature of the zeolite and thus does not represent a marked increase in total Pt electrode surface area, see estimates in Table II. This requires an alternative explanation for the effectiveness of Pt-Y for the dispersion electrolysis of benzene:water over that Pt/Al_2O_3. One explanation is that the conductivity of the dispersion is higher when zeolite particles are present, and thus, the electrolysis is observed atop a large ohmic background. This could arise for two reasons: 1) ion exchange will occur when zeolites are exposed to water since zeolite promotes the autoprotolysis of water due to the exchange reaction of Na^+ in the zeolite for H^+ in solution [15]; and/or more interestingly, 2) under the conditions of dispersion electrolysis the zeolite unit may act as an indissoluble, but mobile solid electrolyte.

Another explanation is that electrolysis is being supported at Pt particles sited in the zeolite interior; Table II shows the immense gain in surface area that is obtained by including the intracrystalline particles. While this latter explanation is desirable from the viewpoint of studying electrode reactions within a zeolite, experiments that will be discussed later show that this possibility is unlikely under the current experimental conditions. A final possibility is that electrode processes do vary due to electrode size and that electrochemical reactivity is greater at the nanometer-sized Pt particles supported on Type Y zeolite.

Conductivity of Water Exposed to Zeolite Type Y

Several control experiments involving only high impedance water were run to gauge the importance of ions exchanging from the zeolite. Water-equilibrated NaY and 1, 5, and 10% Pt-Y were stirred in high impedance water for 30 min and filtered; filtrates were retained to obtain i-V curves using just the Pt feeder electrodes.

Figure 3 presents the results for 30 ml aliquots of filtrate obtained from stirred suspensions of 167 mg of Y zeolite/50 ml H_2O. The i-V curve for high impedance water only (Curve D) shows that the conductivity increases greatly [illegible] exposure to NaY zeolite (Curve B). As anticipated, the increase in conducti[illegible] dependent on the amount of NaY exposed to the solution; using four-fold less [illegible] the suspension step yielded an ohmic response with a 3.5-fold lower slope.

The use of NaY-exposed water as a control is not really valid, however. Forming metal microstructures in zeolites is known to lower the ion-exchange capacity of the modified zeolite [15]. Figure 3C demonstrates that the conductivity of the filtrate obtained after stirring 166 mg 1% Pt-Y_{300} in 50 [illegible] does increase relative to pure water, but the solution conductivity remains [illegible] times lower than an equivalently exposed amount of NaY.

Dispersion Electrolysis of Pure Water

Pt-Y can be used to electrolyze high impedance water only, removing the complicating variable of electroorganic reactions of benzene. Water provides a common reaction medium in which to compare the various forms of supported Pt. Figures 3 and 4 summarize the i-V responses of these dispersed electrode systems.

Figure 3A highlights the dramatic difference in the i-V curves when 1% Pt-Y ultramicroelectrodes are added to the cell. Contrasting this with the appropriate solution background response, Figure 3C, clearly shows that obtaining higher currents at lower voltages was not unique to Pt-Y in benzene:water and is not primarily due to an increase in solution conductivity as ions leach from the zeolite.

Figure 3A also collects the i-V results for the electrolysis of water by dispersed 1% Pt-Y_{300} and 1% Pt-Y_{600} and demonstrates that both forms of 1% Pt-Y respond essentially the same. This result, taken with the XPS results which sh[illegible] that the exterior of 1% Pt-Y_{300} is indistinguishable from that of 1% Pt-Y_{600}, l[illegible] to the conclusion that electrolysis, under present low-field conditions, is supported solely at Pt particles sited on the zeolite exterior.

Pt particles present in the zeolite interior of 1% Pt-Y_{600} should appro[illegible] 2 nm in size, according to Gallezot [35], and thus, be approximately twice th[illegible] size of those in 1% Pt-Y_{300}. Although, the surface area of an individual particle in 1% Pt-Y_{600} is then four-times greater than one in 1% Pt-Y_{300}, the total intracrystalline-sited Pt surface area is just half that in 1% Pt-Y_{300} [41], see Table II.

A two-fold difference in total surface area should be apparent in our i[illegible]

results, but is not, implying that intracrystalline-sited Pt particles are not contributing to the electrolysis; this most probably arises because the applied electric field is insufficient to provide enough of a voltage drop per particle for bipolar electrolysis to occur. Externally sited particles can physically be charged at the feeder electrodes or by other previously charged supported-Pt sites. Lack of reactant in the zeolite interior is a remote possibility in this medium since water sorbs strongly in zeolite.

The lack of electrolytic contribution from interior Pt sites in Pt-Y has also been seen for dispersion electrolyses in neat CH_3CN of ferrocene and a bulky ferrocene derivative too large to enter the zeolite [42]. No difference was observed after normalizing the current responses by correcting for the solution concentrations and diffusion coefficients of the ferrocenyl species, again showing that electrolysis is supported only at Pt particles sited on the zeolite exterior under low-field conditions.

Figure 4 consolidates the i-V responses for the dispersion electrolysis of water at the various forms of supported Pt. For 100 mg samples of Pt-modified support, the electrolytic effectiveness lies in the order 1% Pt-Y > 5% Pt-Y > 10% Pt-Y = 1% Pt/Al_2O_3. Repeating the control experiment of suspending Pt-Y in and analyzing the solution conductance of the filtrate produced Figure 4E, wh the conductivity was identical for 1, 5, and 10% Pt-Y. Again, this ohmic background is greater than pure H_2O, but significantly lower than the electr response seen at 1 and 5% Pt-Y (Curves A and B, respectively) and distinguish from that seen at 10% Pt-Y (Curve D).

Figure 4C shows the effect of "electrolysis" at 1% PtY, the ion-exchange material, and demonstrates that in the absence of metallic Pt on the support, the i-V response is ohmic only. The possibility that dispersed zeolite acts

a solid electrolyte is suggested by the increase in effective conductivity when the ion-exchanged, but non-metallized zeolite particles are dispersed during the i-V measurement at the feeder electrodes. The ohmic response for water + 1% PtY is twice that for water-exposed 1% PtY; compare Figure 4, Curves C and E.

Interestingly, 10% Pt-Y, which is expected to have approximately a 1% weight loading of Pt at its zeolite exterior gave a i-V response indistinguishable from 1% Pt/Al_2O_3, Figure 4D. It is also suggestive that the order of effectiveness for the electrolysis of water matches the general ordering established by XPS for the size of externally sited Pt particles.

Compared to alumina as a support, zeolite offers the ability to sorb small electroactive solutes and electroreaction products, such as the products of water electrolysis, O_2 and H_2. Experiments have been done with H_2 added to the sparging gas during the electrolysis of water at Pt-Y. Only modest increases in current were obtained over that for an inert sparging gas, again indicating that the vast intracrystalline Pt surface area, while H_2-accessible, does not contribute electrochemically. The possibility that pre-concentration of these gaseous reactants by the zeolite might account for the great enhancement in current for 1% Pt-Y over that for 1% Pt/Al_2O_3 in the presence of water prompted a control experiment in which water was electrolyzed at 100 mg 1% Pt/Al_2O_3 and then 100 mg of 5% PtY was added and the i-V curve obtained. The result was a curve like Figure 4D indicating electrolysis, but imposed on the magnitude of Figure 4C for the Pt(II)-exchanged Type Y zeolite; the large currents seen for 1% Pt-Y (Figure 4A) were not observed.

The XPS results can be used to make the following deductions. The particles 1% Pt-Y are on the order of the escape depth of a photoelectron, 2.5-5 nm. exhibits approximately 60% of the Pt intensity expected for this weight loadi

when normalized to the 1% Pt-Y numbers. Making some simplifying assumptions [43] allows a particle size to be estimated for 5% Pt-Y of ~ 20 nm or at least four-times larger than the particles supported on the exterior of 1% Pt-Y. Table II shows that the effective surface area of 20-nm Pt particles externally sited on 5% Pt-Y is greater, but not that dissimilar to that calculated for 5-nm Pt particles externally sited on 1% Pt-Y. However, the electrolytic response is reversed, i.e., more current flows using 1% Pt-Y, the supported-Pt material with less apparent external surface area. This is a preliminary suggestion that electrode processes may be affected by particle size on the submicrometer scale.

Summary

Performing aqueous and two-phase electrolyses between large area (85 cm^2) feeder electrodes in the absence of deliberately added electrolyte salt produces negligible currents, as is appropriate for such high resistance media. Adding a source of supported metal, with an external surface area of the same order of magnitude as the feeder electrodes, produces 10-1000 times more current. Thus, these supported conductors permit electrolyses under low ionic strength conditions where macroelectrodes could not and thereby function as ultramicroelectrodes.

The ability to use supported conductors as dispersed ultramicroelectrodes expands the range of materials that can be explored as ultramicroelectrodes; many of these supported metals or metal oxides are simply prepared or commercially available, e.g., Pt/Al_2O_3 is commercially available and is far less expensive than (unsupported) Pt microspheres. By supporting small particles and using dispersion electrolysis to access them as ultramicroelectrodes, a more efficient use can be made of a frequently expensive electrocatalyst as less material is wasted in the bulk of the structured electrode. This combination also offers a pragmatic

means of realizing electroorganic syntheses in low ionic strength media on a preparative scale.

Zeolite Type Y has been shown to be more effective than alumina as a support for electrolyses with dispersed, supported-Pt ultramicroelectrodes. The control experiments show that although an increase in the conductivity of aqueous-containing media does ensue due to ions exchanged from the zeolite, this higher ohmic background is dwarfed by the electrochemical response obtained in the presence of Pt supported on Type Y zeolite.

A zeolite is an electrical insulator [15], so it should be possible to develop a potential on metals sited in its interior. However, as the dispersion experiment is presently configured, i.e., without separators and at low applied electric fields (<300 V/cm), the Pt particles sited in the zeolite interior are not contributing to the electrolytic effect.

Due to the number of intracrystalline Pt particles in a 0.1 g sample of 1% Pt-Y (8×10^{16} for 1-nm sized particles), and the strong ionic nature of the zeolite matrix (which may partially screen the electric field), fields significantly greater than those used here (<300 V/cm) will be required to achieve bipolar electrolysis at intracrystalline Pt particles. To increase the applied electric field to the point where intracrystalline Pt could experience a voltage sufficient to permit bipolar electrolysis would require suppresssing direct electrolysis at externally sited Pt particles. This could be accomplished by covering each feeder electrode with an ionically conductive polymer and silencing the external Pt particles with a bulky poison, or by using preparatory procedures which sequester the Pt loading in intracrystalline sites only [44].

This successful combination of electrode-modified zeolites and dispersed electrolysis now permits an investigation of the confluence and possible syn-

of electrocatalysis and zeolite catalysis by generating a practical macroscopic output from an ensemble of microscopic sites. The results for dispersion electrolysis at Pt-Y indicate that the electrochemical flux is large (> mA/cm^2) and even in the absence of bipolar electrolysis at intracrystalline Pt, the intrusion of the zeolite on electrode reactions with CE or EC character is anticipated. Supporting ultramicroelectrodes in and on zeolites offers a package to probe fundamental issues concerning ultramicroelectrodes, conductivity, and electrochemical reactivity at scales below 10 nm.

Acknowledgements

The authors would like to thank Dr. Ramanathan Panayappan of the Naval Research Laboratory for performing the DC plasma analyses and Ms. Holly Stewart for analysis of Na^+ by atomic absorption spectrophotometry.

References

1. Murray, R.W. Electroanalytical Chemistry, 13; Bard, A.J., Ed. Dekker: New York, 1984.
2. Wightman, R.M. Anal. Chem. 1981, 53, 1125A.
3. Fleischmann, M.; Pons, S.; Rolison, D.; Schmidt, P.P. Ultramicroelectrodes; Datatech Science: Morganton, NC, 1987.
4. (a) Chidsey, C.E.D.; Feldman, B.J.; Lundgren, C.; Murray, R.W. Anal. Chem. 1986, 58, 601. (b) Geng, L.; Ewing, A.G.; Jernigan, J.C.; Murray, R.W. Anal. Chem. 1986, 58, 852.
5. (a) Kittlesen, G.P.; White, H.S.; Wrighton, M.S. J. Am. Chem. Soc. 1985, 107, 7373; (b) Kittlesen, G.P.; Wrighton, M.S. J. Mol. Electronics 1986, 2, 23, and references therein.
6. Rolison, D.R.; Nowak, R.J.; Pons, S.; Ghoroghchian, J.; Fleischmann, M. Molecular Electronic Devices III; Carter, F.L.; Siatkowski, R.E.; Wohltjen, H. Eds. Elsevier: Amsterdam, in press.
7. Murray, C.G.; Nowak, R.J.; Rolison, D.R. J. Electroanal. Chem. 1984, 164, 205.
8. deVismes, B.; Bedioui, F.; Devynck, J.; Bied-Charreton, C. J. Electroanal. Chem. 1984, 187, 197.
9. (a) Gemborys, H.A.; Shaw, B.R. J. Electroanal. Chem. 1986, 208, 95; (b) Shaw, B.R.; Creasy, K.E.; Lanczycki, C.J.; Sargeant, J.A.; Tirhado, M. J. Electr. Soc. 1988, 135, 0000.
10. Li, Z.; Mallouk, T.E. J. Phys. Chem. 1987, 91, 643.
11. (a) Ghosh, P.K.; Bard, A.J. J. Am. Chem. Soc. 1983, 105, 5691. (b) Ghosh, P.K.; Mau, A.W.H.; Bard, A.J. J. Electroanal. Chem. 1984, 169, 315. (c) [illegible] K.; Bard, A.J. J. Phys. Chem. 1985, 89, 5565; (d) Rudzinski, W.E.; Bard, A. J. Electroanal. Chem. 1986, 199, 323.
12. Kamat, P.V. J. Electroanal. Chem. 1984, 163, 389.

13. (a) Miller, C.J.; Majda, M. J. Am. Chem. Soc. 1985, 107, 1419; (b) Miller, C.J.; Majda, M. J. Electroanal. Chem. 1986, 207, 49.

14. Sinha, S.; Humphrey, B.D.; Fu, E.; Bocarsly, A.B. J. Electroanal. Chem. 1984, 162, 351.

15. Breck, D.W. Zeolite Molecular Sieves; Wiley: New York, 1974.

16. Metal Microstructures in Zeolites; Jacobs, P.A.; Jaeger, N.I.; Jiru, P.; Schulz-Ekloff, G. Eds. Elsevier: Amsterdam, 1982.

17. Fleischmann, M.; Ghoroghchian, J.; Pons, S. J. Phys. Chem. 1985, 89, 5530.

18. Fleischmann, M.; Ghoroghchian, J.; Rolison, D.; Pons, S. J. Phys. Chem. 1986, 90, 6392.

19. Fleischmann, M.; Oldfield, J.W.; Porter, D.F. J. Electroanal. Chem. 1971, 29, 241.

20. Sabacky, B.J.; Evans, J.W. J. Electrochem. Soc. 1979, 126, 1180.

21. Goodridge, F.; King, C.J.H.; Wright, A.B. Electrochim. Acta 1977, 22, 1087.

22. Spiro, M.; Freund, P.L. J. Chem. Soc. Faraday Trans. I 1983, 79, 1649.

23. Freund, P.L.; Spiro, M. J. Phys. Chem. 1985, 89, 1074.

25. Graetzel, M. Faraday Disc. Chem. Soc. 1980, 70, 359.

26. Keller, P.; Mooadpour, A. J. Am. Chem. Soc. 1980, 102, 7193.

27. Meisel, D.; Mulac, W.A.; Matheson, M.S. J. Phys. Chem. 1981, 85, 179.

28. Johansen, O.; Launikouis, A.; Loder, J.W.; Mau, A.S-H.; Sasse, W.H.F.; [illegible] J.D.; Wells, D. Aust. J. Chem. 1981, 34, 981.

29. Miller, D.S.; Bard, A.J.; McLendon, G.; Ferguson, J. J. Am. Chem. Soc. 1981, 103, 5336.

30. Miller, D.S.; McLendon, G. J. Am. Chem. Soc. 1981, 103, 6791.

31. Albery, W.J.; Bartlett, P.M.; McMahon, A.J. Photogeneration of Hydrogen Harriman, A.; West, M.A. Eds. Academic Press: London, 1982.

32. Matheson, M.S.; Lee, P.C.; Meisel, D.; Pelizzetti, E. J. Phys. Chem. 1[illegible] 394.

33. Albery, W.J.; Bartlett, P.N.; McMahon, A.J. J. Electroanal. Chem. 1985, 182, 7.

34. Henglein, A. J. Phys. Chem. 1980, 84, 3461.

35. (a) Gallezot, P.; Alarcon-Diaz, A.; Dalmon, J-A.; Renouprez, A.J.; Imelik, B. J. Catal. 1975, 39, 334; (b) Gallezot, P. Catal. Rev. Sci. Eng. 1979, 20, 121.

36. Winiecki, A.M.; Suib, S.L.; Occelli, M.L. Langmuir 1988, 4, 512.

37. Suib, S.L.; Winiecki, A.M.; Kostapapas, A. Langmuir 1987, 3, 483.

38. Ghoroghchian, J.; Pons, S. private communication, 1986.

39. Wagner, C.D.; Riggs, W.M.; Davis, L.E.; Moulder, J.F.; Muilenberg, G.E. Handbook of X-ray Photoelectron Spectroscopy; Perkin-Elmer Corp., Physical Electronics Division: Eden Prairie, MN, 1979.

40. Fukushima, T.; Katzer, J.R. Proc. of the 7th Int. Congress on Catalysis Seiyama, T.; Tanabe, K. Eds. Elsevier: Amsterdam, 1980.

41. The total particle surface area is ultimately related to the ratio of surface area to volume ($4\pi r^2$:$(4/3)\pi r^3$; see Table IId), when the weight loading, and thus the mass of Pt available to form particles, remains constant, a two-fold increase in particle size relays into a two-fold decrease in total surface area.

42. Rudzinski, W.R.; Rolison, D.R. unpublished results, 1987.

43. The simplifying assumptions are: 1) the supported Pt particles are assumed to be spherical; 2) the supported part of the particle is still "visible" to incident x-rays; 3) an escape depth of 5 nm is assumed; 4) any diminution of photoelectrons emitted by the support atoms due to the loading of Pt (fortunately, a low value at the exterior surface) is neglected. A particle size can then be estimated from the following relationship, knowing that 60% of the expected Pt intensity for 5% Pt-Y (normalized to 1% Pt-Y) was observed and assigning the remaining 40% to a XPS-silent inner core of:

$$\frac{0.6}{1 - 0.6} = \frac{\text{mass visible}}{\text{mass of core}} = \frac{\#\ \text{particles[particle volume - core volume]}}{\#\ \text{particles[core volume]}}$$

Using this approach, the number of particles within the analysis volume need not be known. Defining the radius of the particle as the radius of the XPS-silent core (r_c) plus the escape depth, yields for r in nm:

$$1.5 = [(r_c + 5)^3 - r_c^3]/r_c^3.$$

Solving the resulting cubic equation gives one physically significant root (r_c = 14 nm), for an estimated particle size of 19 nm.

44. Persaud, L.; Bard, A.J.; Campion, A.; Fox, M.A.; Mallouk, T.E.; Webber, S.E.; White, J.M. J. Am. Chem. Soc. 1987, 109, 7309.

TABLE I. X-RAY PHOTOELECTRON DATA: BINDING ENERGIES AND ATOM RATIOS

Sample	(O1s-Si2p)/ev	O1s:(Si2p+Al2s)	$Pt4f_{7/2}$/ev	(Pt4f:Si2p)10^3[a]	Rel.atom% of Pt[b]
NaY	429.0±0.1	1.9+0.1	-	-	-
1% PtY	429.0±0.1	2.0±0.3	73.5±0.6[c]	3.9±0.4	0.08±0.02
5% PtY	428.8±0.4	2.2±0.4	73.4±0.3[c]	18±3	0.37±0.04
10% PtY	429.1±0.1	1.9±0.3	73.1±0.3[c]	40±15	0.9±0.3
1% Pt-Y_{300}	429.2±0.1	2.0±0.3	71.6±0.2	5.2±0.5	0.11±0.01
1% Pt-Y_{600}	429.1±0.1	1.9±0.3	70.8±0.1	5.4±0.4	0.12±0.01
1% Pt-Y[d]	429.1±0.1	2.0±0.2	71.2±0.4	5.3±0.4	0.12±0.01
5% Pt-Y	429.2±0.1	2.2±0.3	71.8±0.2	15.6±0.6	0.34±0.02
10% Pt-Y	429.2±0.1	2.1±0.3	71.7±0.1	24±3	0.57±0.04
1% Pt/Al_2O_3		2.6[e]	70.1	11.0[e]	0.3

[a] One member of the Pt4f doublet could clearly be seen as a shoulder on the Al2p line dependent on the oxidation state of the Pt; see Figure 2. For quantitation, the relative area (obtained after curve fitting) of the more resolved line was used: $Pt4f_{5/2}$ for PtY and $Pt4f_{7/2}$ for Pt-Y.

[b] The relative atom percent of Pt was calculated as the ratio of the relative areas of [Pt4f:(Si2p+Al2s+O1s+Na1s+Pt4f)]x100.

[c] The value for $Pt4f_{7/2}$ is calculated from the value for the more resolved $Pt4f_{5/2}$ line and the known Δ BE($Pt4f_{5/2}$-$Pt4f_{7/2}$) of 3.4 ev [37].

[d] The data sets for 1%Pt-Y_{300} and 1%Pt-Y_{600} were averaged to obtain a representative set of 1%Pt-Y results.

[e] The calculation was made using the relative area of Al2p only.

TABLE II. ESTIMATED ELECTRODE SURFACE AREA IN AN ENSEMBLE OF ULTRAMICROELECTRODES

Sample	Estimated Particle Size/nm[a]	#Pt atoms/particle[b]	"Effective" mass of Pt in 100 mg sample/g[c]	"Effective" Surface Area of Pt in 100 mg sample/cm^2[d]
Pt microspheres	1000	3.5×10^{10}	0.1	280
Pt supported on alumina, 1% w/w	50	4.3×10^{6}	10^{-3}	56
Pt supported on Type Y zeolite,				
1% w/w	5	4300	10^{-4}	56
5% w/w	20	2.8×10^{5}	5×10^{-4}	70
Pt supported within Type Y zeolite,				
1% w/w	1	35	9×10^{-4}	2500
	2	280	9×10^{-4}	1260

[a] A spherical shape is assumed and any blocked surface area due to the support is neglected.

[b] # of Pt atoms/particle = $\frac{(\text{mass of microsphere})N_A}{\text{atomic weight of Pt}} = \frac{(4/3)\pi r^3(\text{density of Pt})6.022 \times 10^{23}}{195.09}$, where the density of Pt is 21.45 g/cm^3 and r is in cm.

[c] For unsupported Pt, all of the sample mass is Pt ; for 100 mg of 1%Pt/Al_2O_3(1g Pt/100g Al_2O_3) only 10^{-3}g of the sample is Pt ; for 1%Pt-Y , the externally sited Pt represents 0.1% of the weight loading , while internally sited Pt is 0.9%.

[d] total surface area = (# of Pt particles) (surface area of 1 particle) = $\frac{\text{Effective Mass}}{\text{Mass of Microsphere}}(4\pi r^2)$, where r is in cm.

Figure Legends

Figure 1: Current-voltage curves for the electrolysis of benzene:water (20ml:8ml) using supported Pt as the dispersed electrodes. A: 103.2 mg 1% $Pt\text{-}Y_{300}$; B: averaged values for two experiments with 100 mg 1% Pt/Al_2O_3, the variance from the mean is less than the height of the symbol; C: 26 mg 1% Pt/Al_2O_3; D: feeder electrodes only.

Figure 2: High resolution XPS scans of the Pt4f/Al2p region for Pt(II)-ion exchanged Zeolite Y before (A, B) and after (C) redox chemistry. A: 1% PtY; B: 5% PtY; C: 1% Pt-Y.

Figure 3: Current-voltage curves in the presence and absence of zeolite-supported Pt ultramicroelectrodes for pure water equilibrated with zeolite. A: i-V response obtained for 1% Pt-Y in 30 ml H_2O after stirring suspension for 30 min, (•) 100.4 mg 1% $Pt\text{-}Y_{600}$, (x) 101.4 mg 1% $Pt\text{-}Y_{300}$; Curves B-D: i-V response with feeder electrodes only; B and C: 30 ml filtrate obtained after stirring suspensions of the following compositions for 30 min; B: 167 mg NaY/50 ml H_2O; C: 166 mg 1% $Pt\text{-}Y_{300}$/50 ml H_2O; D: pure H_2O.

Figure 4: Current-voltage response for the electrolysis of water by 10[illegible] supported Pt dispersed electrodes. A: 1% $Pt\text{-}Y_{600}$; B: 5% Pt-Y; C: 1% PtY (i[illegible] exchanged form, no metallic Pt); D: 10% Pt-Y and 1% Pt/Al_2O_3; E: i-V respo[illegible] feeder electrodes only for 30 ml filtrate obtained after stirring suspensions [illegible] 167 mg 1,5, or 10% Pt-Y/50 ml H_2O.

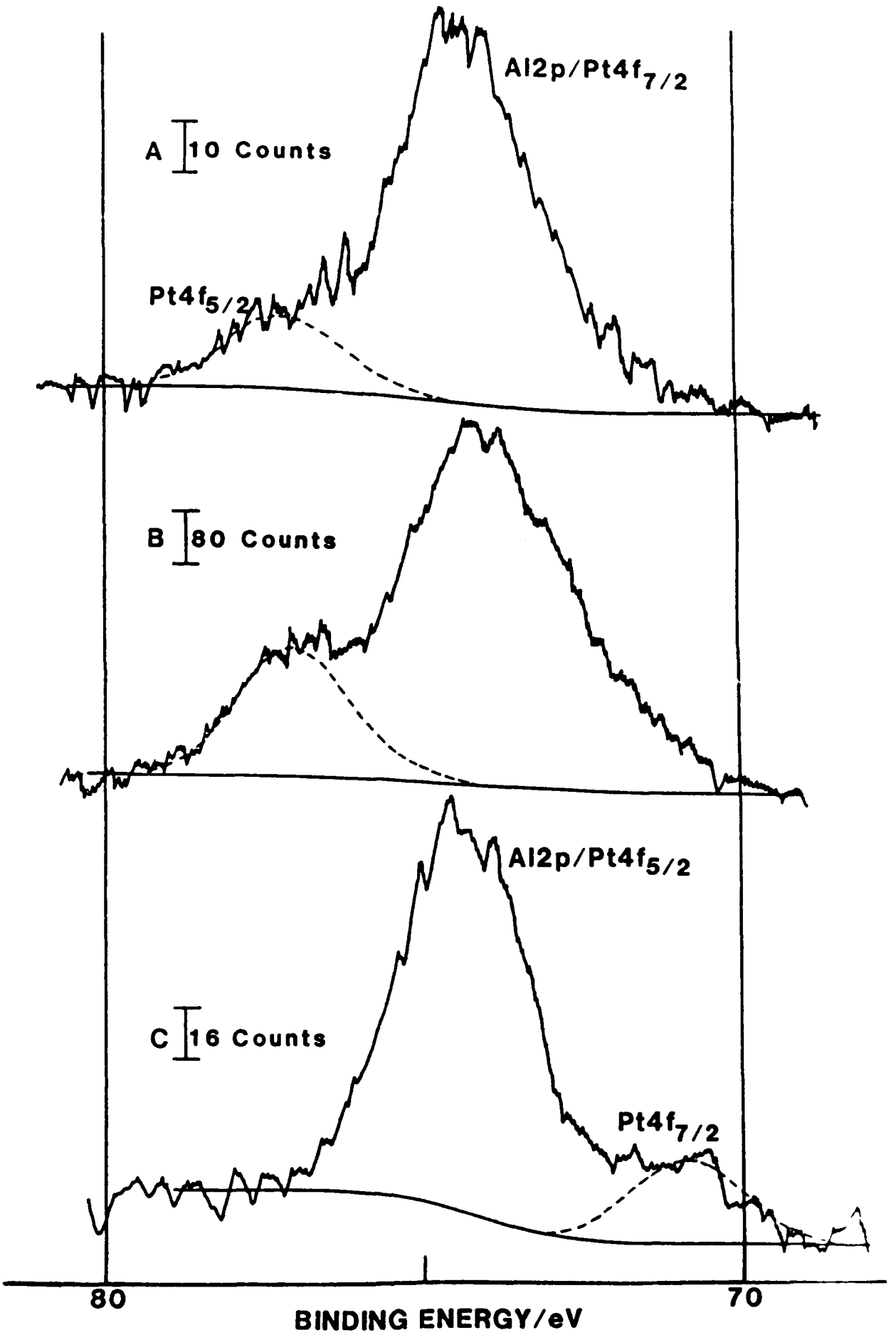
Al2p/Pt4f7/2
A
10 Counts
Pt4f5/2
B
80 Counts
Al2p/Pt4f5/2
C
16 Counts
Pt4f7/2
80
70
BINDING ENERGY/eV

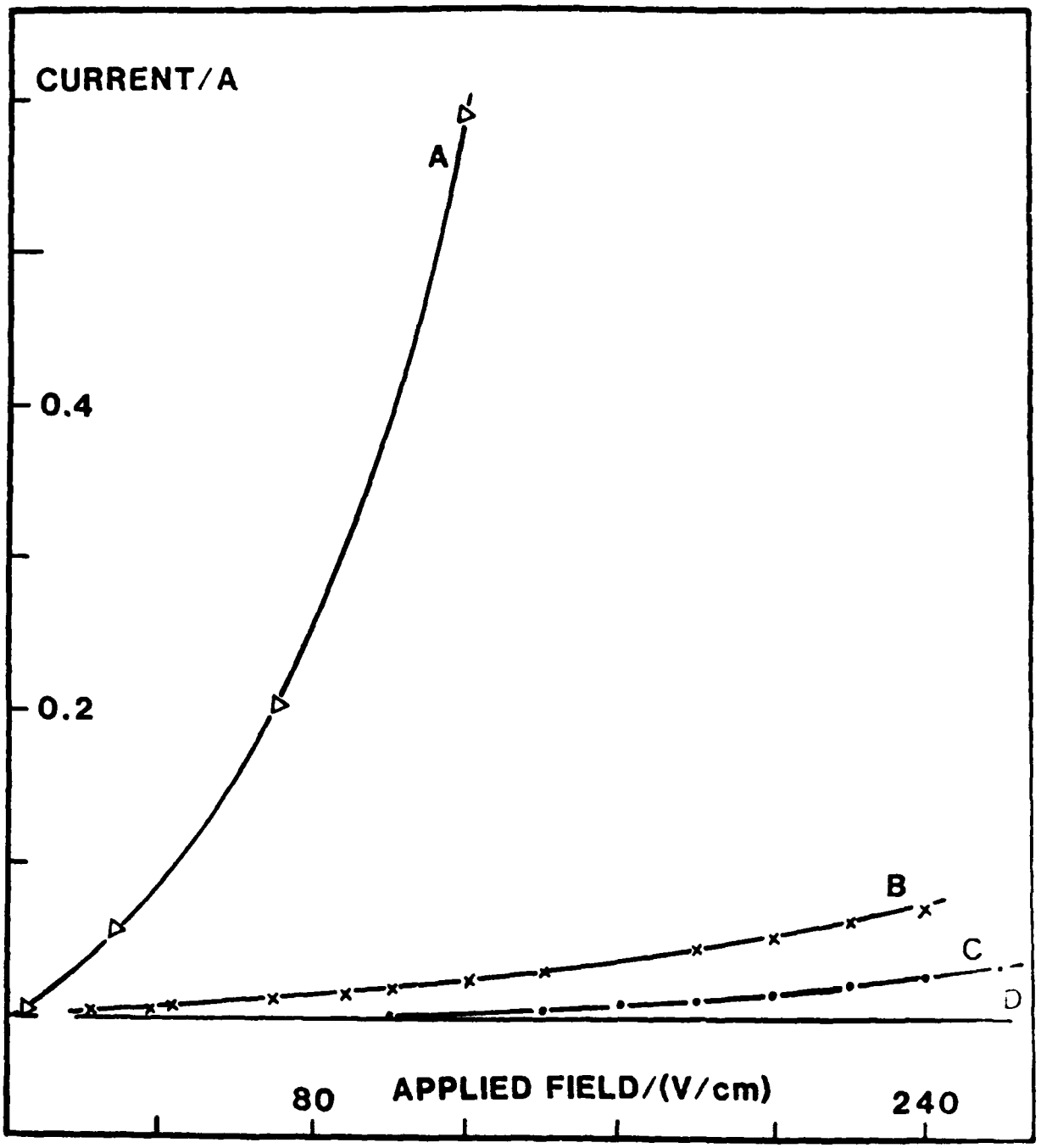
CURRENT/A
0.4
0.2
A
B
C
D
80
APPLIED FIELD/(V/cm)
240

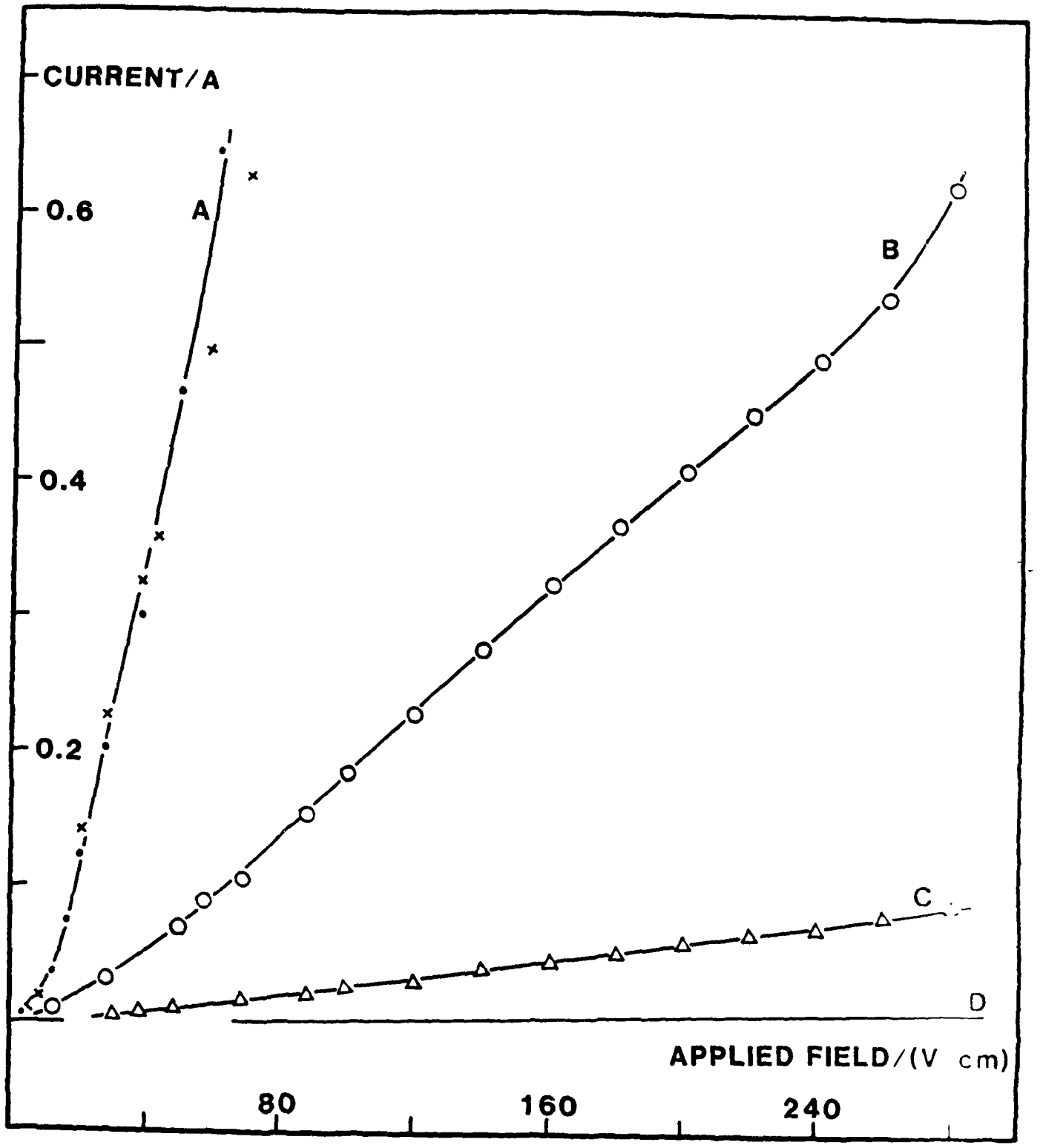
CURRENT/A
0.6
0.4
0.2
A
B
C
D
APPLIED FIELD/(V cm)
80
160
240

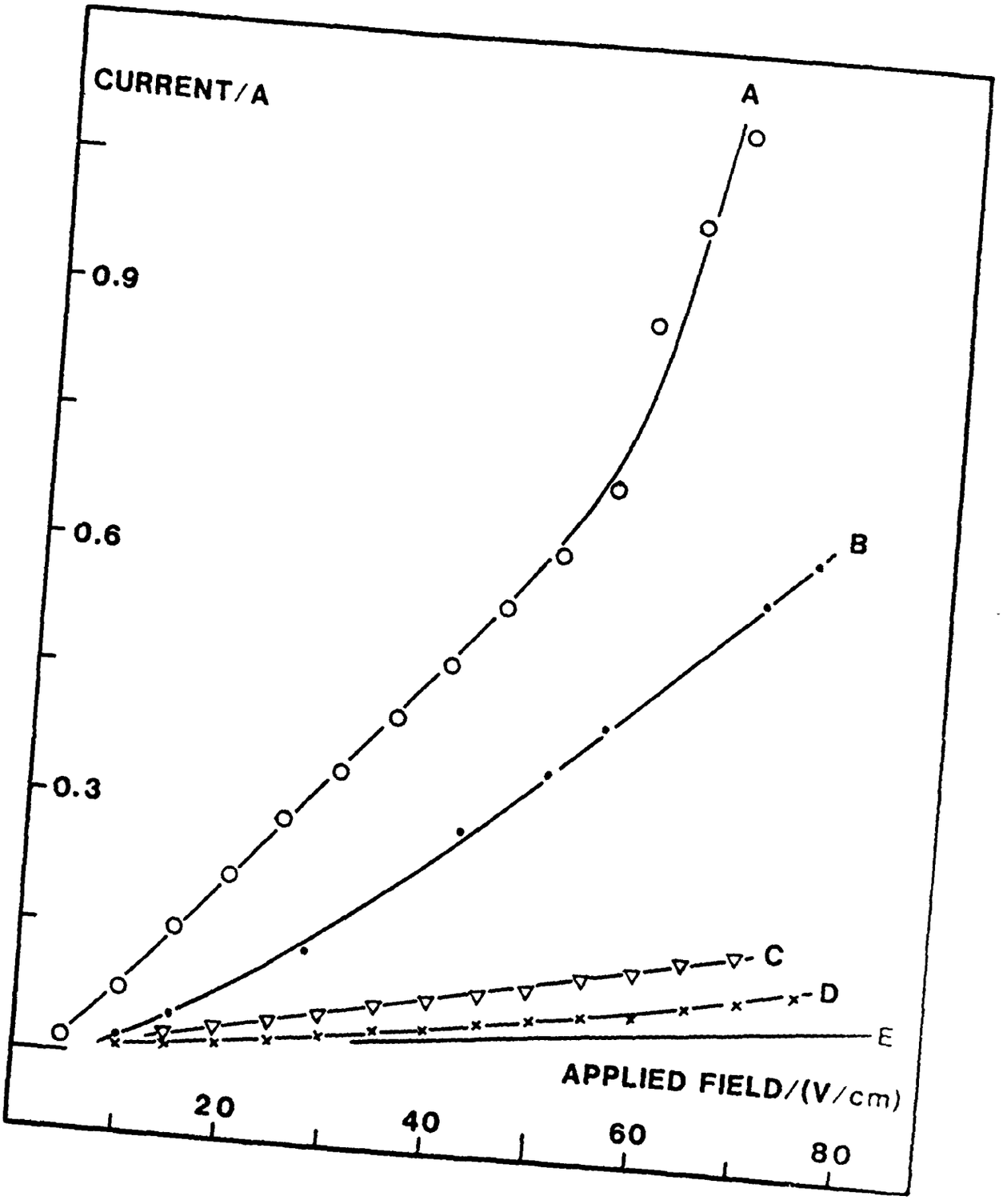
CURRENT/A
A
0.9
0.6
B
0.3
C
D
E
APPLIED FIELD/(V/cm)
20
40
60
80

DL/1113/87/2

TECHNICAL REPORT DISTRIBUTION LIST, GEN

	No. Copies
Office of Naval Research Attn: Code 1113 800 N. Quincy Street Arlington, Virginia 22217-5000	2
Dr. Bernard Douda Naval Weapons Support Center Code 50C Crane, Indiana 47522-5050	1
Naval Civil Engineering Laboratory Attn: Dr. R. W. Drisko, Code L52 Port Hueneme, California 93401	1
Defense Technical Information Center Building 5, Cameron Station Alexandria, Virginia 22314	12 high quality
DTNSRDC Attn: Dr. H. Singerman Applied Chemistry Division Annapolis, Maryland 21401	1
Dr. William Tolles Superintendent Chemistry Division, Code 6100 Naval Research Laboratory Washington, D.C. 20375-5000	1
Dr. David Young Code 334 NORDA NSTL, Mississippi 39529	1
Naval Weapons Center Attn: Dr. Ron Atkins Chemistry Division China Lake, California 93555	1
Scientific Advisor Commandant of the Marine Corps Code RD-1 Washington, D.C. 20380	1
U.S. Army Research Office Attn: CRD-AA-IP P.O. Box 12211 Research Triangle Park, NC 27709	1
Mr. John Boyle Materials Branch Naval Ship Engineering Center Philadelphia, Pennsylvania 19112	1
Naval Ocean Systems Center Attn: Dr. S. Yamamoto Marine Sciences Division San Diego, California 91232	1

ABSTRACTS DISTRIBUTION LIST, SDIO/IST

Dr. Robert A. Osteryoung
Department of Chemistry
State University of New York
Buffalo, NY 14214

Dr. Douglas N. Bennion
Department of Chemical Engineering
Brigham Young University
Provo, UT 84602

Dr. Stanley Pons
Department of Chemistry
University of Utah
Salt Lake City, UT 84112

Dr. H. V. Venkatasetty
Honeywell, Inc.
10701 Lyndale Avenue South
Bloomington, MN 55420

Dr. J. Foos
EIC Labs Inc.
111 Downey St.
Norwood, MA 02062

Dr. Neill Weber
Ceramatec, Inc.
163 West 1700 South
Salt Lake City, UT 84115

Dr. Subhash C. Narang
SRI International
333 Ravenswood Ave.
Menlo Park, CA 94025

Dr. J. Paul Pemsler
Castle Technology Corporation
52 Dragon Ct.
Woburn, MA 01801

Dr. R. David Rauh
EIC Laboratory Inc.
111 Downey Street
Norwood, MA 02062

Dr. Joseph S. Foos
EIC Laboratories, Inc.
111 Downey Street
Norwood, Massachusetts 02062

Dr. Donald M. Schleich
Department of Chemistry
Polytechnic Institute of New York
333 Jay Street
Brooklyn, New York 01

Dr. Stan Szpak
Code 633
Naval Ocean Systems Center
San Diego, CA 92152-5000

Dr. George Blomgren
Battery Products Division
Union Carbide Corporation
25225 Detroit Rd.
Westlake, OH 44145

Dr. Ernest Yeager
Case Center for Electrochemical Science
Case Western Reserve University
Cleveland, OH 44106

Dr. Mel Miles
Code 3852
Naval Weapons Center
China Lake, CA 93555

Dr. Ashok V. Joshi
Ceramatec, Inc.
2425 South 900 West
Salt Lake City, Utah 84119

Dr. W. Anderson
Department of Electrical & Computer Engineering
SUNY - Buffalo
Amherst, Massachusetts 14260

Dr. M. L. Gopikanth
Chemtech Systems, Inc.
P.O. Box 1067
Burlington, MA 01803

Dr. H. F. Gibbard
Power Conversion, Inc.
495 Boulevard
Elmwood Park, New Jersey 07407

DL/1113/87/2

ABSTRACTS DISTRIBUTION LIST, SDIO/IST

Dr. V. R. Koch
Covalent Associates
52 Dragon Court
Woburn, MA 01801

Dr. Randall B. Olsen
Chronos Research Laboratories, Inc.
4186 Sorrento Valley Blvd.
Suite H
San Diego, CA 92121

Dr. Alan Hooper
Applied Electrochemistry Centre
Harwell Laboratory
Oxfordshire, OX11 ORA UK

Dr. John S. Wilkes
Department of the Air Force
The Frank J. Seiler Research Lab.
United States Air Force Academy
Colorado Springs, CO 80840-6528

Dr. Gary Bullard
Pinnacle Research Institute, Inc.
10432 N. Tantan Avenue
Cupertino, CA 95014

Dr. J. O'M. Bockris
Ementech, Inc.
Route 5, Box 946
College Station, TX 77840

Dr. Michael Binder
Electrochemical Research Branch
Power Sources Division
U.S. Army Laboratory Command
Fort Monmouth, New Jersey 07703-5000

Professor Martin Fleischmann
Department of Chemistry
University of Southampton
Southampton, Hants, SO9 5NH UK